IRIS AperTO

UNIVERSITÀ DEGLI STUDI DI TORINO

AperTO - Archivio Istituzionale Open Access dell'Università di Torino

An FGFR3 autocrine loop sustains acquired resistance to trastuzumab in gastric cancer patients

This is the author's manuscript

Original Citation:

Availability:

This version is available http://hdl.handle.net/2318/1621544 since 2017-05-15T15:50:13Z

Published version:

DOI:10.1158/1078-0432.CCR-16-0178

Terms of use:

Open Access

Anyone can freely access the full text of works made available as "Open Access". Works made available under a Creative Commons license can be used according to the terms and conditions of said license. Use of all other works requires consent of the right holder (author or publisher) if not exempted from copyright protection by the applicable law.

(Article begins on next page)

05 November 2024

IRIS AperTO

UNIVERSITÀ DEGLI STUDI DI TORINO

This is the author's final version of the contribution published as:

Piro, Geny; Carbone, Carmine; Cataldo, Ivana; Di Nicolantonio, Federica; Giacopuzzi, Simone; Aprile, Giuseppe; Simionato, Francesca; Boschi, Federico; Zanotto, Marco; Mina, Maria Mihaela; Santoro, Raffaela; Merz, Valeria; Sbarbati, Andrea; de Manzoni, Giovanni; Scarpa, Aldo; Tortora, Giampaolo; Melisi, Davide. An FGFR3 autocrine loop sustains acquired resistance to trastuzumab in gastric cancer patients. CLINICAL CANCER RESEARCH. 2016; 22 (24) pp: 6164-6175.
DOI: 10.1158/1078-0432.CCR-16-0178

The publisher's version is available at:
http://clincancerres.aacrjournals.org/content/22/24/6164.full-text.pdf

When citing, please refer to the published version.

Link to this full text:
http://hdl.handle.net/2318/1621544

This full text was downloaded from iris - AperTO: https://iris.unito.it/

iris - AperTO

University of Turin's Institutional Research Information System and Open Access Institutional Repository

An FGFR3 autocrine loop sustains acquired resistance to trastuzumab in gastric cancer patients

Geny Piro[1,2,*], Carmine Carbone[1*], Ivana Cataldo[3], Federica Di Nicolantonio[4], Simone Giacopuzzi[5], Giuseppe Aprile[6], Francesca Simionato[9], Federico Boschi[7], Marco Zanotto[1], Maria Mihaela Mina[2], Raffaela Santoro[1], Valeria Merz[9], Andrea Sbarbati[8], Giovanni de Manzoni[5], Aldo Scarpa[3], Giampaolo Tortora[2, 9], and Davide Melisi[1, 9]

[1]Digestive Molecular Clinical Oncology Research Unit, Department of Medicine, Università degli studi di Verona, Verona, Italy; [2]Laboratory of Oncology and Molecular Therapy, Department of Medicine, Università degli studi di Verona, Verona, Italy; [3]ARC-Net Research Centre and Department of Pathology and Diagnostics, Università degli studi di Verona, Verona, Italy; [4]Department of Oncology, University of Turin, Italy, and Candiolo Cancer Institute – FPO, IRCCS, Candiolo, Torino, Italy; [5]Esophageal and gastric Surgery Unit, Department of Surgery, Azienda Ospedaliera Universitaria Integrata, Verona, Italy; [6]Department of Medical Oncology, Azienda Ospedaliero-Universitaria, Udine, Italy; [7]Department of Computer Science, Università degli studi di Verona, Verona, Italy; [8]Section of Anatomy and Histology, Department of Neurological, Neuropsychological, Morphological and Movement Sciences, Università degli studi di Verona, Verona, Italy; [9]Medical Oncology Unit, Azienda Ospedaliera Universitaria Integrata, Verona, Italy.

[*]*These authors contributed equally to this work*

Running Title: FGFR3 in trastuzumab-resistant gastric cancer

Keywords: FGFR3; trastuzumab; resistance; gastric cancer

Financial Support: This work was supported in part by the Associazione Italiana per la Ricerca sul Cancro (AIRC) Start-Up n°10129, and 5 per mille n°10016 to DM, and by the AIRC grants IG 11930, 5 per mille 12182, 12214, and PRIN n°2009X23L78_005 to GT. Partial support was also provided by grant Farmacogenomica' 5 per mille 2009 MIUR from Fondazione Piemontese per la Ricerca sul Cancro—ONLUS to FDN and Fondo per la Ricerca Locale (ex 60%), Università di Torino, 2014 to FDN.

Disclosure of Potential Conflicts of Interest: No potential conflicts of interest to disclose.

Corresponding author: Davide Melisi, MD, PhD, Digestive Molecular Clinical Oncology Research Unit, Section of Medical Oncology, Department of Medicine, Università degli studi di Verona, Piazzale L.A. Scuro, 10, 37134, Verona, Italy; phone: +39 045 812 8148; fax: +39 045 802; email: davide.melisi@univr.it

TRANSLATIONAL RELEVANCE

The majority of gastric cancer patients who achieve an initial response to trastuzumab-based regimens develop resistance within 1 year of treatment. The molecular mechanisms involved in trastuzumab-resistance of gastric cancer remain uncharacterized. In the present study, we propose an in vivo model in which trastuzumab therapy induces the selection of gastric cancers overexpressing FGFR3, which activates the PI3K/AKT/mTOR signaling pathway, sustaining, in turn, tumor growth and a more aggressive EMT phenotype. We confirmed our finding by demonstrating for the first time the overexpression of FGFR3 in paired pretreatment and postprogression bioptic samples from patients affected by advanced gastric cancer that relapsed upon trastuzumab therapy. Of translational relevance, we showed the therapeutic efficacy in vivo of the FGFR3 inhibitor dovitinib in models of trastuzumab-resistant gastric cancer. Our study provides the preclinical rationale to investigate the inhibition of FGFR3 as second-line treatment strategy in gastric cancer patients refractory to first-line trastuzumab-containing therapies.

ABSTRACT

Purpose: The majority of gastric cancer patients who achieve an initial response to trastuzumab-based regimens develop resistance within 1 year of treatment. This study was aimed at identifying the molecular mechanisms responsible for resistance.

Experimental Design: A $HER2^{+}$- trastuzumab sensitive NCI-N87 gastric cancer orthotopic nude mouse model was treated with trastuzumab until resistance emerged. Differentially expressed transcripts between trastuzumab-resistant and sensitive gastric cancer cell lines were annotated for functional interrelatedness by Ingenuity Pathway Analysis software. Immunohistochemical analyses were performed in pre- vs. post-treatment biopsies from gastric cancer patients receiving trastuzumab-based treatments. All statistical tests were two-sided.

Results: Four NCI-N87 trastuzumab resistant (N87-TR) cell lines were established. Microarray analysis showed HER2 downregulation, induction of epithelial-to-mesenchymal transition, and indicated fibroblast growth factor receptor 3 (FGFR3) as one of the top upregulated genes in N87-TR cell lines. *In vitro*, N87-TR cell lines demonstrated a higher sensitivity than did trastuzumab-sensitive parental cells to the FGFR3 inhibitor dovitinib, which reduced expression of pAKT, ZEB1, and cell migration. Oral dovitinib significantly (P= 0.0006) reduced tumor burden and prolonged mice survival duration in N87-TR mouse models. A higher expression of FGFR3, phosphorylated AKT, and ZEB1 were observed in biopsies from patients progressing under trastuzumab-based therapies if compared with matched pre-treatment biopsies.

Conclusions: This study identified the FGFR3/AKT axis as an escape pathway responsible for trastuzumab resistance in gastric cancer, thus indicating the inhibition of FGFR3 as a potential strategy to modulate this resistance.

INTRODUCTION

Gastric cancer is the fourth most commonly diagnosed cancer and the third leading cause of cancer-related death worldwide (1, 2). Trastuzumab – a recombinant humanized monoclonal antibody directed against the human epidermal growth factor receptor 2 (HER2) – is the only targeted agent to be approved for the first line treatment of patients with HER2-overexpressing metastatic gastric or gastroesophageal junction adenocarcinoma (3). However, after an initial period of clinical benefit, patients almost inevitably progress, as the tumors become refractory to trastuzumab (4).

Several mechanisms involved in acquired resistance to trastuzumab have been described in breast cancer (5), including overexpression of Cyclin E (6), cross-talk between HER2 and other tyrosine kinase receptors (7, 8), or activation of downstream intracellular signal transducers such as SRC (9).

By contrast, the molecular mechanisms involved in resistance to trastuzumab in gastric cancer remain largely uncharacterized. Recently, integrated SNP-array-based copy number and whole-exome sequencing analyses of data from HER2-amplified gastroesophageal adenocarcinoma revealed that more than half of the cases had additional oncogenic alterations at diagnosis that could potentially hamper the antitumor effect of anti-HER2 agents, including amplifications of cell-cycle related genes *CCNE1* and *CDK6*, PI3K pathway activation by *PI3KCA* mutations, and gene amplification of other tyrosine kinase receptors such as *EGFR* and *MET* (10).

Solid cancers are molecularly heterogeneous, but among the large number of genetic alterations present at diagnosis only few of them represent relevant driver gene mutations that directly or indirectly confer a selective growth advantage (11). Although we recognize the potential contributions of additional oncogenic alterations present at diagnosis to tumor progression during therapy with trastuzumab, a number of genes that contain few or no mutations could be instead overexpressed, down-regulated, or epigenetically altered, thus playing an equally important role in the development of drug resistance (12).

Therefore, in the present study we aimed at directly identifying transcriptional mechanisms responsible for the resistance of gastric cancer to trastuzumab, which may represent new therapeutic targets in the search for ways to reverse the invariable escape of this disease from anti- HER2 therapies.

MATERIALS AND METHODS

Cell Lines, Reagents and In Vitro Studies

Human gastric cancer cell line NCI-N87 and human breast cancer cell lines MCF-7 and BT474 were obtained from ATCC (Manassas, VA, USA). Human gastric cancer cell line YCC-2 was obtained from KCLB (Seoul, Korea). Cell lines were authenticated by standard short tandem repeat (STR) DNA typing methodology before being purchased from cell bank. Cells were daily checked by morphology and routinely tested to be Mycoplasma free by PCR assay. Generation of Green-Fluorescent-Protein+/luciferase+ NCI-N87 cell line (13), *in vitro* cell proliferation assay, wound-healing assay (14), immunohistochemistry, protein extraction and Western blotting (15) were performed as previously described, and for further details see Supplementary Materials and Methods.

Gene Expression Microarray and Pathway Analysis

RNA isolation and quantitative RT-PCR assay were performed as detailed in Supplementary Materials and Methods. Differences in gene expression between parental and resistant cells were examined using Illumina Human 48k-gene-chips (Illumina, Milan, Italy) as indicated in Supplementary Materials and Methods. Gene expression microarray data have been deposited in the GEO database (accession number GSE77346). Differentially expressed transcripts were tested for network and functional interrelatedness using the IPA software program (Ingenuity Systems, Redwood, CA).

Establishment of Gastric Cancer Cell Lines In Vivo Resistant to Trastuzumab and In Vivo Studies

Six- to eight-week-old female BALB/c athymic (nu/nu) mice were purchased from Harlan Laboratories (Indianapolis, Indiana). All mice were housed and treated in accordance with the guidelines of the Italian Ministry of Health Animal Care and Use Committee, and maintained in specific pathogen-free conditions at CIRSAL Animal Care Facility (Verona, Italy). The orthotopic

implantation of gastric cancer cells was performed in six mice as described previously (16). Briefly, green fluorescent protein+/luciferase+ NCI-N87 cell line was harvested from sub-confluent culture by exposure to trypsin. Trypsinization was stopped with medium containing 10% Fetal Bovine Serum, and the cells were washed once with Phosphate Buffered Saline (PBS). To produce orthotopic gastric tumors, $1x10^6$ cells resuspended in 50 µl of PBS/matrigel solution (1:1) were injected into the gastric wall of nude mice anesthetized with a 1.5% isoflurane–air mixture. To prevent such leakage, a cotton swab was held over the injection site for 1 minute. One layer of the abdominal wound was closed with wound clips (Auto-clip; Clay Adams, Parsippany, NJ). The mice tolerated the surgical procedure well, and no anesthesia-related deaths occurred. Tumor growth was monitored by Bioluminescent imaging performed using a cryogenically cooled IVIS 100 imaging system coupled with a data-acquisition computer running the Living Image software program (Xenogen, Hopkinton, MA). When the resulting tumors became detectable, the mice were given 20 mg/kg of trastuzumab intraperitoneally (i.p.) twice a week until the tumors suddenly recurred during continuous therapy. Treatment resistance developed in 4 out of 6 mice. At evidence of advanced bulky disease, mice were euthanized using carbon dioxide inhalation. Four trastuzumab-resistant cell lines were established from excised tumors via repeated green fluorescent protein flow cytometric sorting with FACSAria II sorter (Becton Dickinson, Franklin Lakes, New Jersey, USA).

The subcutaneous heterotopic implantation of gastric cancer cells was performed as described previously (17). Tumor bearing mice were randomly assigned (n = 10 per group) to receive 20mg/Kg of trastuzumab i.p. twice a week for four weeks, or 40 mg/kg of dovitinib oral gavage daily for four weeks, or respective vehicles as a control. Tumor size was measured with a caliper by the modified ellipsoid formula $(\pi/6) \times AB^2$ where A is the longest and B is the shortest perpendicular axis of an assumed ellipsoid corresponding to tumor mass. All mice were weighed weekly and observed for tumor growth. When at least six of the ten mice in a treatment group presented with bulky disease, the median survival duration for that group was considered to have been reached. At the median survival duration of the control group, the tumor growth in mice in all groups was evaluated. The mice were euthanized using carbon dioxide inhalation when evidence of advanced

bulky disease developed or at cut-off volume of 2 cm^3, which was considered the day of death for the purpose of survival evaluation.

Patients

Three patients were considered for analyses. For each patient, pre- and post-resistance tumor samples were compared by immunohistochemical analyses. Informed consent was obtained from all patients. See Supplementary Materials and Methods for clinical history and details.

Statistical Analysis

The results of in vitro proliferation were analyzed for statistical significance of differences by nonlinear regression analysis and are expressed as means and 95% confidence intervals [CIs] for at least three independent experiments performed in quadruplicate. Statistical significance of differences in tumor growth was determined by the Mann–Whitney test; differences in survival duration were determined using a log-rank test. All statistical tests were two-sided, and a P value less than .05 indicated statistical significance. All statistical analyses were performed using GraphPad Prism software version 4.0c for Macintosh (GraphPad Software, San Diego, CA).

RESULTS

In Vivo Selection of Four Gastric Cancer Models with Acquired Resistance to Trastuzumab

We initially measured the expression levels of several members of the EGFR protein family in YCC-2 and NCI-N87 gastric cancer, and in the BT-474 and MCF-7 breast cancer cell lines (19), used as HER2-positive and negative controls, respectively. NCI-N87 gastric cancer cells showed a high basal expression of HER2 comparable to that of the HER2-positive BT-474 breast cancer cells. (Figure 1, A). Consistently with the expression of HER2, the NCI-N87 and BT-474 cells demonstrated *in vitro* a significantly higher sensitivity to trastuzumab (NCI-N87 IC_{50}= 4.74 μg/mL; BT-474 IC_{50}= 1.05 μg/mL) than did YCC-2 and MCF-7 cells (IC_{50}> 400 μg/mL) (Figure 1, B).

In order to study the molecular mechanisms of acquired resistance to HER2 targeted agents in gastric cancer, we established and validated four novel trastuzumab-resistant cell lines, N87-TR1, N87-TR2, N87-TR3 and N87-TR4 (Figure 1, C). Trastuzumab-resistant cell lines had a more spindle-shaped morphology (Figure 1, D) and exhibited significantly higher migration rates compared with trastuzumab-sensitive NCI-N87 (*P*<.001) (Supplementary Figure 1).

N87-TR1, N87-TR2, N87-TR3 and N87-TR4 cells demonstrated a significantly higher resistance *in vitro* to trastuzumab than did the parental NCI-N87 cells (NCI-N87 IC_{50}= 4.74 μg/mL vs. N87-TR1, N87-TR2, N87-TR3 or N87-TR4 IC_{50}> 400 μg/mL) (Figure 1, E). As expected, NCI-N87 tumors were sensitive to drug treatment, whereas mice bearing trastuzumab-resistant tumors had survival rates comparable to untreated control mice (Figure 1, F).

Identification of Relevant Biological Processes and Genes by Using Global Transcript Profiling

To gain insight into the molecular mechanisms underlying trastuzumab– resistant phenotype in gastric cancer cells, we compared gene expression profiles in sensitive and resistant cells by microarray analysis in order to identify groups of genes associated with a specific signaling

pathway or biological process. Differentially modulated transcripts in trastuzumab–resistant cells were enriched for genes implicated in mammalian target of rapamycin (mTOR) signaling pathway and regulation of the eukaryotic initiation factors (eIFs) 2 and 4 (Figure 2, A). Top differentially regulated transcripts in trastuzumab–resistant gastric cancer cell lines compared with NCI-N87 control cell line are summarized in Supplementary Table 1.

Down-regulation of HER2, EGFR and HER3 expression in trastuzumab-resistant lines was evident, which was confirmed at the protein level by Western blot (Figure 2, B). Consistent with this finding, while trastuzumab blocked the activation of AKT in sensitive NCI-N87 cells, it was completely ineffective in trastuzumab-resistant lines (Supplementary Figure 2).

On the other hand, transcriptome analysis revealed that the expression of ZEB1, a key member of the transcriptional complexes essential for the development of the epithelial- to-mesenchymal transition (EMT) genetic program, and that of the mesenchymal marker vimentin (*VIM*) were strongly upregulated, and that the expression of the epithelial marker gene E-cadherin (*CDH1*) was strongly downregulated in trastuzumab–resistant gastric cancer cell lines compared with sensitive control cell line (Supplementary Table 1, and Figure 2, C). Consistently, the N87-TR1, N87-TR2, N87-TR3, and N87-TR4 cell lines had considerably lower levels of E-cadherin and higher levels of ZEB1 and vimentin protein expression than did their trastuzumab–sensitive cell lines when cultured *in vitro* (Figure 2, D). These results indicate EMT as a plausible underlying molecular mechanism responsible for the phenotypic changes observed in trastuzumab resistant cells.

Among the top differentially regulated genes, we also found a consistent overexpression of the membrane receptor gene *FGFR3* and of the gene coding for its ligand FGF9 in the N87-TR1, N87-TR2, N87-TR3, and N87-TR4 trastuzumab–resistant gastric cancer cell lines compared with NCI-N87 sensitive control cell lines (Figure 2, E). We validated that resistant cell lines had significantly higher levels of FGFR3, and of total and phosphorylated AKT then did their trastuzumab-sensitive parental counterparts. On the other hand, in all trastuzumab-resistant lines we found a profound suppression of basal ERK1/2 phosphorylation, the other main intracellular signaling pathway activated by tyrosine kinase receptors (Figure 2, F).

We corroborated the most relevant changes in protein levels *in vivo*. All trastuzumab-resistant tumors had undetectable or low levels of HER2 expression. NCI-N87 tumors had low expression levels of FGFR3 and of phosphorylated AKT, high expression of E-cadherin and no expression of ZEB1 and vimentin. In contrast, all trastuzumab-resistant tumors exhibited a significantly stronger expression of FGFR3 and phosphorylated AKT, no expression of E-cadherin, but high expression levels of ZEB1 and vimentin (Figure 3).

Based on the overall results, we propose a mechanistic model for the resistance to trastuzumab in gastric cancer in which an autocrine loop established through the overexpression of FGFR3 and of its ligand FGF9 could be responsible for the activation of the PI3K/AKT/mTOR signaling pathway, sustaining, in turn, tumor growth and EMT irrespectively of the anti-HER2 treatment (Figure 2G).

Effects of FGFR inhibition in Trastuzumab-Resistant Gastric Cancer Models

In order to validate our proposed model, we tested the activity of two different FGFR3 inhibitors, dovitinib and AZD4547 in vitro. All four trastuzumab-resistant cell lines were significantly more sensitive than NCI-N87 parental cells (dashed line) to the same extent to the inhibition of FGFR3 (All $P<.0001$) (Figure 4, A). Furthermore, we found that in a clinically relevant concentration range, dovitinib was able to induce a measurable reduction of the phosphorylation of AKT (Figure 4, B), suppressed the expression of ZEB1 (Figure 4, C), and significantly ($P<.01$) inhibited migration in all trastuzumab-resistant cell lines (Figure 4, D - E).

To demonstrate that FGFR3 is a druggable target to overcome acquired resistance to trastuzumab in gastric cancer, 40 mice were injected with trastuzumab-sensitive NCI-N87 or trastuzumab-resistant N87-TR4 gastric cancer cells and randomly assigned to receive oral dovitinib or its vehicle as a control. Dovitinib was completely inactive in NCI-N87 tumor bearing mice (Figure 5, A). Conversely, N87-TR4 gastric cancer bearing mice treated with dovitinib experienced a significant reduction in tumor burden. Accordingly, only the N87-TR4 tumor bearing mice treated with dovitinib demonstrated a significantly longer median survival duration ($P= 0.0006$) (Figure 5, B). In this regard, control N87-TR4 tumors from mice treated with oral vehicle

showed a moderate to strong expression of phosphorylated AKT. Conversely, N87-TR4 tumors from mice treated with dovitinib demonstrated only very weak or no expression of phosphorylated AKT (Figure 5, C).

Validation of the FGFR3/AKT Axis As An Escape Pathway For Trastuzumab Resistance In Gastric Cancer Patients

In order to corroborate the clinical relevance of our findings, we identified three patients affected by advanced gastric cancer who received trastuzumab-containing treatments, and for which there were available both pretreatment and postprogression bioptic samples. The clinical history for each patient is depicted in Figure 6. Immunohistochemical analyses were performed on both pretreatment and postprogression samples to determine the expression of FGFR3, activated AKT, and of the EMT marker ZEB1. We demonstrated that in all three patients, samples taken at trastuzumab progression exhibited significantly higher FGFR3 expression than their matched pretreatment samples. Consistently, we observed higher expression levels of activated AKT and ZEB1 in postprogression bioptic samples when compared with their respective pretreatment samples (Figure 6).

DISCUSSION

In this study, we sought to identify the molecular mechanisms responsible for the resistance of gastric cancer to anti-HER2 treatment trastuzumab. We demonstrated that trastuzumab induces the selection of gastric cancer cells overexpressing FGFR3 and its specific ligand FGF9. This autocrine loop activates the PI3K/AKT/mTOR signaling pathway, sustaining, in turn, tumor growth and a more aggressive EMT phenotype. To our knowledge, this is the first study to provide evidences that targeting the kinase activity of FGFR3 could be a valid approach to modulate acquired resistance to trastuzumab in gastric cancer.

FGFR3 is a member of a family of four tyrosine kinase receptors that contribute to carcinogenesis by stimulating tumor proliferation, survival and neoangiogenesis (20). Recent studies provide evidence for an increasing role or FGFR signaling as a key mediator of resistance to several anticancer therapies (21, 22), including the dual HER2 and EGFR inhibitor lapatinib (23). In our study, we demonstrated that FGFR3 is overexpressed in gastric cancer tumor models selected for resistance to trastuzumab. Most importantly, we confirmed our finding by demonstrating for the first time the overexpression of FGFR3 in paired pretreatment and postprogression bioptic samples from patients affected by advanced gastric cancer that relapsed upon therapies with trastuzumab.

FGF9 is one of the members of the heparin binding polypeptide ligands of the FGF family, which presents a unique affinity (kd: 0.25 nM) for FGFR3 (24). FGF9 was initially identified as an important secreted mediator for the epithelial to mesenchymal cell signaling during embryonic development (25). In this present study, we measured a significantly higher expression of FGF9 in trastuzumab–resistant gastric cancer cell lines than in the sensitive parental line, thus supporting the existence of an autocrine loop between FGF9 and overexpressed FGFR3.

Either the interaction of FGFR3 with the specific ligand FGF9 or the ligand-independent dimerization induced by the overexpression of FGF receptors may lead to the transphosphorylation of their tyrosine kinase domains, activating, in turn, the MAPK and the PI3K/AKT/mTOR signaling pathways (20). The continued activation of the PI3K/AKT/mTOR signaling pathway is the most

common alteration associated with the resistance to anti-HER2 therapies in breast cancer (26, 27). More recent clinical evidences suggested that activating mutations in the *PI3KCA* gene encoding the p110a catalytic subunit of the PI3K enzyme (28, 29), rather than the loss or inactivating mutations of phosphatase and tensin homologue on chromosome 10 (*PTEN*) (30), might be important biomarkers to identify breast cancer patients resistant to anti-HER2 therapies. However, less is know about the role of FGFR pathway in anti-HER2 resistance in breast cancer. It has been demonstrated that FGFR2 is a pivotal molecule for the survival of lapatinib resistant cells, suggesting that a switch of addiction from the HER2 to the FGFR2 pathway enable cancer cells to become resistant to HER2-targeted therapy (23). In our study, we demonstrated that the AKT signaling pathway is significantly activated in trastuzumab-resistant gastric cancer models if compared with sensitive control. More significantly, we demonstrated for the first time the over activation of the AKT signaling pathway in postprogression bioptic samples from gastric cancer patients receiving therapies with trastuzumab if compared with their respective pretreatment samples. Most importantly, we demonstrated that the over activation of the AKT signaling pathway in trastuzumab-resistant gastric cancer models is dependent on the overexpression of FGFR3 and can be modulated by the inhibition of this receptor.

EMT is a transdifferentiation process that converts tumor cells with an epithelial phenotype into highly motile mesenchymal cells (31). The PI3K/AKT/mTOR signaling pathway demonstrated an essential role in mediating EMT, thought the activation of both mTOR complex 1 (mTORC1) (32), and mTORC2 (33, 34) In our study, we found an EMT phenotype and increased cell motility in trastuzumab-resistant gastric cancer models. We demonstrated that the induction of this phenotype parallels the over activation of the AKT signaling pathway, and is sustained by the autocrine loop between overexpressed FGF9 and FGFR3 as it can be modulated by the FGFR3 inhibitor dovitinib. Of clinical relevance, we showed for the first time the over expression of the EMT marker ZEB1 in postprogression bioptic samples from gastric cancer patients receiving therapies with trastuzumab if compared with their respective pretreatment samples.

Dovitinib (TKI258, Novartis) is a multitargeted receptor tirosine kinase inhibitor, which strongly binds to FGFR3 and inhibits its phosphorylation [NCI Drug Dictionary]. This agent is currently

explored as a monotherapy in the second and third-line setting [NCT01719549], and in combination with docetaxel in the second-line setting [NCT01921673] for patients with gastric cancer. In our study, we showed that dovitinib significantly reduced the activation of AKT and the expression of ZEB1, inhibiting, in turn, the growth and the migratory properties of trastuzumab resistant cells. Of translational relevance, we showed the therapeutic efficacy of treatment with dovitinib in an in vivo model of trastuzumab-resistant N87-TR4 gastric cancer xenografts.

This study, however, had some limitations. The orthotopic xenograft tumor models used are limited by the artificial microenvironment in an immune compromised host and could not faithfully recapitulate the histopatologic features of the human disease, thus, impairing the representativeness of the results observed to human patients. Moreover, the four different TR cell lines developed and analyzed in this study derive from NCI-N87 cells, thus, we could not exclude that different mechanisms of resistance could have been emerged by starting the selection process from different HER2-positive gastric cancer cell models. In this regard, we corroborated the clinical relevance of our findings for human gastric cancer patients by detecting for the first time a significantly higher expression of FGFR3, activated AKT, and of the EMT marker ZEB1 in post-treatment biopsies when compared with their respective pre-treatment biopsies from three gastric cancer patients receiving trastuzumab-based treatments. The limited number of patients' samples available and the potential heterogeneity in the primary tumor and among the different sites of metastasis analyzed could represent additional potential limitations of this study.

Two prior studies reported the development of trastuzumab-resistant NCI-N87 cells (35, 36). Eto and colleagues established a resistant cell line by culturing NCI-N87 cells *in vitro* in the presence of increasing concentration of trastuzumab from 5 to 100 μg/mL along 6 months (35). Similarly, Yang and colleagues selected in vitro another resistant cell line by growing NCI-N87 over a one-year period in increasing concentration of trastuzumab up to 10 μg/mL. During the development of the resistance, NCI-N87 cells underwent EMT, as shown by the increase of ZEB1 expression and of their migratory properties. However, trastuzumab was still able to suppress the phosphorylation of AKT in this cell model, and the activation of an IL6/STAT3/Jagged-1/Notch positive feedback

signaling loop was indicated as associated with the acquisition of trastuzumab resistance (36). In our study, we developed four different trastuzumab-resistant models through, not an in vitro, but an in vivo process of selection by using a clinically relevant model of orthotopic growth of tumors in the mouse stomach. We verified the resistance of these models to trastuzumab in vitro up to 400 μg/mL, as well as in vivo. Whereas we confirmed the acquisition of an EMT phenotype and an overexpression of ZEB1 in the trastuzumab-resistant models when compared with sensitive cells, we did not measure any significant overexpression of IL6 or Jagged-1 in our models (data not shown).

In conclusion, we propose a model in which trastuzumab induces the selection of gastric cancer cells overexpressing FGFR3 and its ligand FGF9. This autocrine signaling loop sustains the activation of the PI3K/AKT/mTOR signaling pathway, and in turn, tumor growth and a more aggressive EMT phenotype. Most importantly, our study provides the preclinical rationale to investigate the inihibition of FGFR3 as second-line treatment strategy in gastric cancer patients refractory to first-line trastuzumab-containing therapies.

Acknowledgments

We thank Licia Montagna for the technical execution of immunohistochemistry. Part of the work was performed at the Laboratorio Universitario di Ricerca Medica (LURM) Research Center, University of Verona.

References

1. Siegel RL, Miller KD, Jemal A. Cancer statistics, 2015. CA: a cancer journal for clinicians. 2015;65:5-29.

2. Lordick F, Allum W, Carneiro F, Mitry E, Tabernero J, Tan P, et al. Unmet needs and challenges in gastric cancer: the way forward. Cancer Treat Rev. 2014;40:692-700.

3. Bang YJ, Van Cutsem E, Feyereislova A, Chung HC, Shen L, Sawaki A, et al. Trastuzumab in combination with chemotherapy versus chemotherapy alone for treatment of HER2-positive advanced gastric or gastro-oesophageal junction cancer (ToGA): a phase 3, open-label, randomised controlled trial. Lancet. 2010;376:687-97.

4. Aprile G, Giampieri R, Bonotto M, Bittoni A, Ongaro E, Cardellino GG, et al. The challenge of targeted therapies for gastric cancer patients: the beginning of a long journey. Expert Opin Investig Drugs. 2014;23:925-42.

5. Tortora G. Mechanisms of resistance to HER2 target therapy. Journal of the National Cancer Institute Monographs. 2011;2011:95-8.

6. Scaltriti M, Eichhorn PJ, Cortes J, Prudkin L, Aura C, Jimenez J, et al. Cyclin E amplification/overexpression is a mechanism of trastuzumab resistance in HER2+ breast cancer patients. Proc Natl Acad Sci U S A. 2011;108:3761-6.

7. Huang X, Gao L, Wang S, McManaman JL, Thor AD, Yang X, et al. Heterotrimerization of the growth factor receptors erbB2, erbB3, and insulin-like growth factor-i receptor in breast cancer cells resistant to herceptin. Cancer Res. 2010;70:1204-14.

8. Ritter CA, Perez-Torres M, Rinehart C, Guix M, Dugger T, Engelman JA, et al. Human breast cancer cells selected for resistance to trastuzumab in vivo overexpress epidermal growth factor receptor and ErbB ligands and remain dependent on the ErbB receptor network. Clin Cancer Res. 2007;13:4909-19.

9. Zhang S, Huang WC, Li P, Guo H, Poh SB, Brady SW, et al. Combating trastuzumab resistance by targeting SRC, a common node downstream of multiple resistance pathways. Nat Med. 2011;17:461-9.

10. Kim J, Fox C, Peng S, Pusung M, Pectasides E, Matthee E, et al. Preexisting oncogenic events impact trastuzumab sensitivity in ERBB2-amplified gastroesophageal adenocarcinoma. J Clin Invest. 2014;124:5145-58.

11. Vogelstein B, Papadopoulos N, Velculescu VE, Zhou S, Diaz LA, Jr., Kinzler KW. Cancer genome landscapes. Science. 2013;339:1546-58.

12. Melisi D, Piro G, Tamburrino A, Carbone C, Tortora G. Rationale and clinical use of multitargeting anticancer agents. Curr Opin Pharmacol. 2013;13:536-42.

13. Carbone C, Tamburrino A, Piro G, Boschi F, Cataldo I, Zanotto M, et al. Combined inhibition of IL1, CXCR1/2, and TGFbeta signaling pathways modulates in-vivo resistance to anti-VEGF treatment. Anti-cancer drugs. 2016;27:29-40.

14. Carbone C, Piro G, Fassan M, Tamburrino A, Mina MM, Zanotto M, et al. An angiopoietin-like protein 2 autocrine signaling promotes EMT during pancreatic ductal carcinogenesis. Oncotarget. 2015;6:13822-34.

15. Raben D, Bianco C, Damiano V, Bianco R, Melisi D, Mignogna C, et al. Antitumor activity of ZD6126, a novel vascular-targeting agent, is enhanced when combined with ZD1839, an epidermal growth factor receptor tyrosine kinase inhibitor, and potentiates the effects of radiation in a human non-small cell lung cancer xenograft model. Mol Cancer Ther. 2004;3:977-83.

16. Sumida T, Kitadai Y, Shinagawa K, Tanaka M, Kodama M, Ohnishi M, et al. Anti-stromal therapy with imatinib inhibits growth and metastasis of gastric carcinoma in an orthotopic nude mouse model. Int J Cancer. 2011;128:2050-62.

17. Rosa R, Melisi D, Damiano V, Bianco R, Garofalo S, Gelardi T, et al. Toll-like receptor 9 agonist IMO cooperates with cetuximab in K-ras mutant colorectal and pancreatic cancers. Clin Cancer Res. 2011;17:6531-41.

18. Melisi D, Caputo R, Damiano V, Bianco R, Veneziani BM, Bianco AR, et al. Zoledronic acid cooperates with a cyclooxygenase-2 inhibitor and gefitinib in inhibiting breast and prostate cancer. Endocr Relat Cancer. 2005;12:1051-8.

19. Isola J, Chu L, DeVries S, Matsumura K, Chew K, Ljung BM, et al. Genetic alterations in ERBB2-amplified breast carcinomas. Clin Cancer Res. 1999;5:4140-5.

20. Touat M, Ileana E, Postel-Vinay S, Andre F, Soria JC. Targeting FGFR Signaling in Cancer. Clin Cancer Res. 2015;21:2684-94.

21. Oliveras-Ferraros C, Cufi S, Queralt B, Vazquez-Martin A, Martin-Castillo B, de Llorens R, et al. Cross-suppression of EGFR ligands amphiregulin and epiregulin and de-repression of FGFR3 signalling contribute to cetuximab resistance in wild-type KRAS tumour cells. Br J Cancer. 2012;106:1406-14.

22. Yadav V, Zhang X, Liu J, Estrem S, Li S, Gong XQ, et al. Reactivation of mitogen-activated protein kinase (MAPK) pathway by FGF receptor 3 (FGFR3)/Ras mediates resistance to vemurafenib in human B-RAF V600E mutant melanoma. J Biol Chem. 2012;287:28087-98.

23. Azuma K, Tsurutani J, Sakai K, Kaneda H, Fujisaka Y, Takeda M, et al. Switching addictions between HER2 and FGFR2 in HER2-positive breast tumor cells: FGFR2 as a potential target for salvage after lapatinib failure. Biochem Biophys Res Commun. 2011;407:219-24.

24. Hecht D, Zimmerman N, Bedford M, Avivi A, Yayon A. Identification of fibroblast growth factor 9 (FGF9) as a high affinity, heparin dependent ligand for FGF receptors 3 and 2 but not for FGF receptors 1 and 4. Growth factors. 1995;12:223-33.

25. Colvin JS, White AC, Pratt SJ, Ornitz DM. Lung hypoplasia and neonatal death in Fgf9-null mice identify this gene as an essential regulator of lung mesenchyme. Development. 2001;128:2095-106.

26. Berns K, Horlings HM, Hennessy BT, Madiredjo M, Hijmans EM, Beelen K, et al. A functional genetic approach identifies the PI3K pathway as a major determinant of trastuzumab resistance in breast cancer. Cancer Cell. 2007;12:395-402.

27. Nagata Y, Lan KH, Zhou X, Tan M, Esteva FJ, Sahin AA, et al. PTEN activation contributes to tumor inhibition by trastuzumab, and loss of PTEN predicts trastuzumab resistance in patients. Cancer Cell. 2004;6:117-27.

28. Majewski IJ, Nuciforo P, Mittempergher L, Bosma AJ, Eidtmann H, Holmes E, et al. PIK3CA mutations are associated with decreased benefit to neoadjuvant human epidermal growth factor receptor 2-targeted therapies in breast cancer. J Clin Oncol. 2015;33:1334-9.

29. Loibl S, von Minckwitz G, Schneeweiss A, Paepke S, Lehmann A, Rezai M, et al. PIK3CA mutations are associated with lower rates of pathologic complete response to anti-human epidermal growth factor receptor 2 (her2) therapy in primary HER2-overexpressing breast cancer. J Clin Oncol. 2014;32:3212-20.

30. Nuciforo PG, Aura C, Holmes E, Prudkin L, Jimenez J, Martinez P, et al. Benefit to neoadjuvant anti-human epidermal growth factor receptor 2 (HER2)-targeted therapies in HER2-positive primary breast cancer is independent of phosphatase and tensin homolog deleted from chromosome 10 (PTEN) status. Ann Oncol. 2015;26:1494-500.

31. Lamouille S, Xu J, Derynck R. Molecular mechanisms of epithelial-mesenchymal transition. Nat Rev Mol Cell Biol. 2014;15:178-96.

32. Lamouille S, Derynck R. Cell size and invasion in TGF-beta-induced epithelial to mesenchymal transition is regulated by activation of the mTOR pathway. J Cell Biol. 2007;178:437-51.

33. Gulhati P, Bowen KA, Liu J, Stevens PD, Rychahou PG, Chen M, et al. mTORC1 and mTORC2 regulate EMT, motility, and metastasis of colorectal cancer via RhoA and Rac1 signaling pathways. Cancer Res. 2011;71:3246-56.

34. Lamouille S, Connolly E, Smyth JW, Akhurst RJ, Derynck R. TGF-beta-induced activation of mTOR complex 2 drives epithelial-mesenchymal transition and cell invasion. J Cell Sci. 2012;125:1259-73.

35. Eto K, Iwatsuki M, Watanabe M, Ishimoto T, Ida S, Imamura Y, et al. The sensitivity of gastric cancer to trastuzumab is regulated by the miR-223/FBXW7 pathway. Int J Cancer. 2015;136:1537-45.

36. Yang Z, Guo L, Liu D, Sun L, Chen H, Deng Q, et al. Acquisition of resistance to trastuzumab in gastric cancer cells is associated with activation of IL-6/STAT3/Jagged-1/Notch positive feedback loop. Oncotarget. 2015;6:5072-87.

Figure Legends

Figure 1. In vivo selection of gastric cancer models with acquired resistance to trastuzumab treatment. **A)** Western blot analysis for the expression of ErbB family receptors in breast cancer, MCF-7 and BT-474, and gastric cancer, YCC-2 and NCI-N87 cell lines. **B)** Percent relative growth of MCF-7 and BT-474 breast cancer, and YCC-2 and NCI-N87 gastric cancer cell lines, 72h after treatment with increasing concentrations of trastuzumab. Vehicle–treated cells were assigned a value of 100% and designated as control. Means and 95% confidence intervals of three independent experiments performed in quadruplicate are shown. **C)** Green fluorescent protein^{+}/luciferase^{+} NCI-N87 cells were orthotopically injected into the gastric wall of four nude mice. When the resulting tumors became detectable, the mice were given 20 mg/kg of trastuzumab intraperitoneally (i.p.) twice a week. As expected, the tumors responded dramatically to the treatment. The mice received treatment until the tumors suddenly recurred during continuous therapy with trastuzumab. At evidence of advanced bulky disease, mice were euthanized. Four novel trastuzumab-resistant cell lines – N87-TR1, N87-TR2, N87-TR3 and N87-TR4 – were established from excised tumors via repeated green fluorescent protein flow cytometric sorting. The tumor growth was quantified weekly on the basis of bioluminescence emitted by the tumor cells as the sum of all detected photons within the region of the tumor per second using a cryogenically cooled IVIS 100 imaging system coupled with a data-acquisition computer running the Living Image software program (Xenogen, Hopkinton, MA). A digital grayscale image was acquired, followed by the acquisition and overlay of a pseudocolor image representing the spatial distribution of detected photons emerging from the active luciferase within the mouse (representative image). **D)** Light- and fluorescent microscopic phenotype of the trastuzumab-sensitive NCI-N87 cells and trastuzumab-resistant N87-TR1, N87-TR2, N87-TR3 and N87-TR4 gastric cancer cells. **E)** Percent relative growth of trastuzumab-sensitive NCI-N87 cells and trastuzumab-resistant N87-TR1, N87-TR2, N87-TR3 and N87-TR4 gastric cancer cells, 72h after treatment with increasing concentrations of trastuzumab. Vehicle–treated cells were assigned a value of 100% and designated as control. Means and 95% confidence intervals of three

independent experiments performed in quadruplicate are shown. **F)** Fifty athymic nude mice bearing heterotopic NCI-N87, N87-TR1, N87-TR2, N87-TR3 and N87-TR4 gastric tumors were randomly assigned to 10 groups (n=5 per group) to receive 20 mg/kg of either trastuzumab or saline (control) i.p. twice a week. Mice were sacrificed by carbon dioxide inhalation when evidence of advanced bulky disease developed. The day of sacrifice was considered the day of death from disease for the purpose of survival evaluation. Differences among survival duration of mice in each group were determined by log-rank test. NCI-N87, control vs. trastuzumab, median survival = 66.5 vs. undefined days, *P*= 0.0027 hazard ratio= 0.03652, 95% CI= 0.004217 to 0.3163; N87-TR1, control vs trastuzumab, median survival= 55 vs. 49 days, hazard ratio= 0.7026, 95% CI= 0.04055 to 12.17, *P*= 0.8; N87-TR2, control vs. trastuzumab, median survival= 54 vs. 42.5 days, hazard ratio= 1.338, 95% CI= 0.3258 to 5.491, *P*= 0.686; N87-TR3, control vs. trastuzumab, median survival= 49 vs 40 days, hazard ratio= 3.621, 95% CI= 0.5385 to 19.75, *P*= 0.1983; N87-TR4, control vs. trastuzumab, median survival= 54.5 vs 44 days, hazard ratio= 2.143, 95% CI= 0.2905 to 15.8, *P*= 0.4547.

Figure 2. Identification of relevant biological processes and genes by using global transcript profiling. **A)** Signaling pathways enriched among genes differentially expressed in trastuzumab resistant gastric cancer cells versus their sensitive control cell line. The X-axis represents the -log (10) P value for enrichment, with the threshold drawn at P = 0.05. **B)** Western blot analysis for the expression of ErbB family receptors in N87-TR gastric cancer cells compared to trastuzumab-sensitive NCI-N87 gastric cancer and BT-474 breast cancer cells, and trastuzumab-resistant YCC2 gastric cancer and MCF-7 breast cancer cells. **C)** Validation of ZEB-1, E-cadherin (CDH1), and vimentin (VIM) genes differentially expressed in trastuzumab-resistant cells vs parental sensitive cells. Quantitative real time PCR data are expressed as the fold change in RNA expression between the gene of interest and β-actin. Mean and 95% confidence intervals are shown. **D)** Western blot analysis for the expression of epithelial-to-mesenchymal transition markers. **E)** Validation of fibroblast growth factor (FGF)9 and FGF receptor 3 (FGFR3) genes differentially expressed in trastuzumab-resistant cells vs parental sensitive cells. Quantitative real time PCR

data are expressed as the fold change in RNA expression between the gene of interest and β-actin. Mean and 95% confidence intervals are shown. **F)** Western blot analysis for the expression of FGFR3, and the activation of AKT and ERK1/2, in N87-TR cells and their control cell line. **G)** Interaction network derived from genes upregulated in trastuzumab–resistant gastric cancer cell lines versus the respective sensitive control cell line. Each interaction is supported by at least one literature reference identified in the Ingenuity Pathway Knowledge Base, with solid lines representing direct interactions and dashed lines representing indirect interactions. FGFR3: Fibroblast Growth Factor Receptor 3; FGF9: Fibroblast Growth Factor 9; PIP2: Phosphatidylinositol 4,5-bisphosphate; PIP3: Phosphatidylinositol (3,4,5)-trisphosphate; AKT: V-Akt Murine Thymoma Viral Oncogene Homolog; PI3K: Phosphatidylinositol-4,5-Bisphosphate 3-Kinase; PDK1: Pyruvate Dehydrogenase Kinase Isozyme 1; CDH1: Cadherin 1; TSC1: Tuberous Sclerosis 1; TSC2: Tuberous Sclerosis 2; Rheb: RAS-Homolog Enriched in Brain; mTORC1: Mechanistic Target Of Rapamycin Complex 1; mTORC2: Mechanistic Target Of Rapamycin Complex 2; Rho: Rhodopsin; Rock: Rho-Associated Coiled-Coil Containing Protein Kinase; VIM: vimentin; Raptor: Regulatory Associated Protein Of MTOR Complex 1; GBL: G protein beta subunit-like; PRAS40: proline-rich Akt substrate of 40 kDa; mTOR: mammalian target of rapamycin; Rictor: RPTOR Independent Companion Of MTOR Complex 2; Proctor: Protein observed with Rictor-1; SIN1: SAPK-Interacting Protein.

Figure 3. Immunohistochemical analysis of trastuzumab resistant vs trastuzumab sensitive gastric xenograft tumors. Serial paraffin-embedded tumor sections were stained with antibodies against HER2, fibroblast growth factor receptor 3 (FGFR3), ZEB1, pAKT, E-cadherin and vimentin proteins (scale bar: 200 micron; 10x magnification).

Figure 4. In vitro antitumor activity of fibroblast growth factor receptor 3 inhibitor dovitinib in trastuzumab resistant N87-TR cell lines. **A)** Percent relative growth of N87-TR cells and their control cell line, 72h after treatment with increasing concentrations of dovitinib or AZD4547. Vehicle–treated cells were assigned a value of 100% and designated as control. Means and 95%

confidence intervals of three independent experiments performed in quadruplicate are shown. Dovitinib: NCI-N87 IC_{50}= 2.189E-006 M vs. N87-TR1 IC_{50}= 4.122E-007 M, or vs. N87-TR2 IC_{50}= 5.297E-007 M, N87-TR3 IC_{50}= 6.127E-007 M, N87-TR4 IC_{50}= 5.764E-007 M, All *P*<.0001; AZD4547: NCI-N87 IC_{50}= 1.697E-005 M vs. N87-TR1 IC_{50}= 1.038E-005 M, or vs. N87-TR2 IC_{50}= 9.465E-006 M, N87-TR3 IC_{50}= 9.161E-006 M, N87-TR4 IC_{50}= 6.875E-006 M, All *P*<.0001 **B)** Western blot analysis for the activation of AKT after 24h treatment with dovitinib. **C)** Western blot analysis for the expression of ZEB1 after 72h treatment with dovitinib. **D)** Photographs of the wound area were taken by using phase-contrast microscopy immediately and 36 hours after the incision in untreated and treated cells. **E)** Levels of cancer cell migration of N87-TR cells and their control cell line after dovitinib treatment. Results are presented as percentages of the total distances between the wound edges enclosed by cancer cells. The mean values and 95% confidence intervals from 3 independent experiments done in quadruplicate are shown. Relative migration: NCI-N87, control, mean= 15.91, 95%CI= 12.75 to 19.06, vs. dovitinib, mean=8.39, 95%CI= 5.24 to 11.55, P<.01; N87-TR1, control, mean= 93.85, 95%CI= 86.05 to 101.65, vs. dovitinib, mean= 3.51, 95%CI= 1.84 to 5.17, P<.001; N87-TR2, control, mean= 100, 95%CI= 99.12 to 100.88, vs. dovitinib, mean= 4.41, 95%CI= 3.53 to 5.28, P<.001; N87-TR3, control, mean= 93.84, 95%CI= 85.42 to 102.25, vs. dovitinib, mean= 4.06, 95%CI= 2.14 to 5.99, P<.001; N87-TR4, control, mean= 100, 95%CI= 99.12 to 100.88, vs. dovitinib, mean= 6.33, 95%CI= 5.11 to 7.55, P<.001. **, P < 0.01; *** P < 0.001 (unpaired Student's t test) .

Figure 5. Antitumor activity of oral fibroblast growth factor receptor 3 inhibitor dovitinib in vivo in N87-TR4 and NCI-N87 gastric tumor xenografts. **A)** and **B)** Left, forty athymic nude mice bearing subcutaneous heterotopic NCI-N87 or N87-TR4 gastric tumors were randomly assigned to four groups (n= 10 per group) to receive daily oral dovitinib (40 mg/Kg) or vehicle for 4 weeks. Mice were sacrificed by carbon dioxide inhalation when reached cut-of volume of $2cm^3$. The day of sacrifice was considered the day of death from disease for the purpose of survival evaluation. Differences among survival duration of mice in each group were determined by log-rank test. Right, tumor growth at the median survival duration of the control group (65 and 40 days for NCI-N87 and

N87-TR4 respectively). Error bars are 95% confidence intervals. (NCI-N87 tumor volume: control, mean= 1921 mm^3, 95%CI= 1836 to 2007; dovitinib, mean= 1813, 95%CI= 1574 to 2051; survival: control vs dovitinib, median survival = 65 vs 62 days, hazard ratio= 0.7750, 95% CI = 0.2664 to 2.255, *P*= 0.64) (N87-TR4 tumor volume: control, mean= 1910, 95%CI= 1459 to 2362; dovitinib, mean= 1086, 95%CI= 803 to 1369; survival: control vs dovitinib, median survival = 40 vs 63 days, hazard ratio= 0.1413, 95% CI = 0.04611 to 0.4331, *P*= 0.0006). **C)** Six mice bearing N87-TR4 gastric tumors were randomly allocated (n= 3 per group) to receive 40 mg/kg daily oral dovitinib or vehicle as control. Treatments were continued for 4 weeks. Tumors were excised 1 day after the end of treatments. Paraffin-embedded gastric tumor sections stained immunohistochemically with antibodies against pAKT.

Figure 6. Analysis of pre- treatment and post- progression biopsies from gastric cancer patients and clinical history. Paraffin- embedded sections from patients treated with trastuzumab who underwent relapse were immunohistochemically stained with antibodies against fibroblast growth factor receptor 3 (FGFR3), p-AKT, and ZEB1. (scale bar: 200 micron; 10x magnification).

Figure 1.

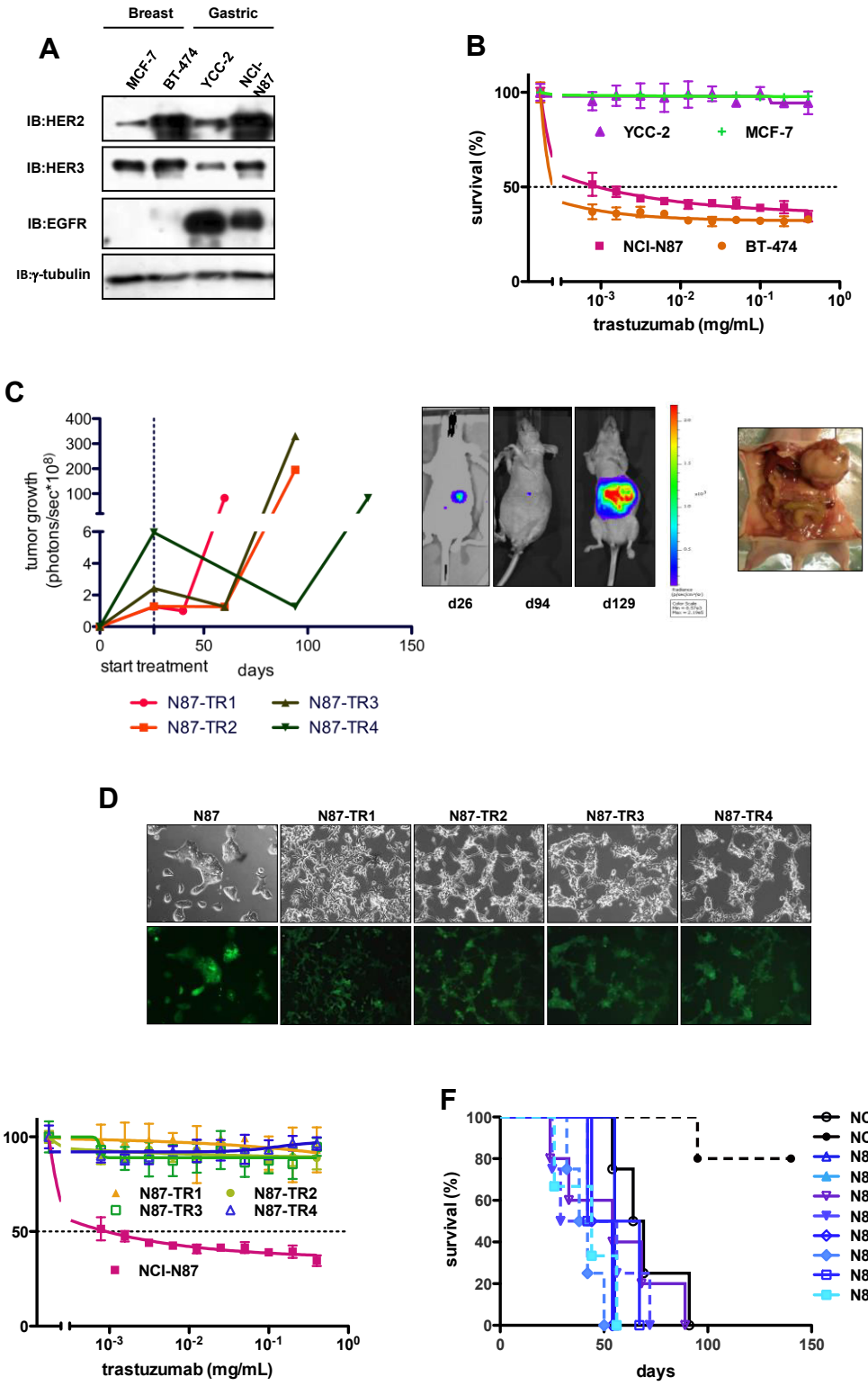
A
Breast
Gastric
MCF-7
BT-474
YCC-2
NCI-N87
IB:HER2
IB:HER3
IB:EGFR
IB:γ-tubulin
B
survival (%)
YCC-2
MCF-7
NCI-N87
BT-474
trastuzumab (mg/mL)
C
tumor growth (photons/sec*10^8)
start treatment
days
N87-TR1
N87-TR2
N87-TR3
N87-TR4
d26
d94
d129
D
N87
N87-TR1
N87-TR2
N87-TR3
N87-TR4
E
survival (%)
N87-TR1
N87-TR2
N87-TR3
N87-TR4
NCI-N87
trastuzumab (mg/mL)
F
survival (%)
days
NCI-N87 + vehicle
NCI-N87 + trastuzumab
N87-TR1 + vehicle
N87-TR1 + trastuzumab
N87-TR2 + vehicle
N87-TR2 + trastuzumab
N87-TR3 + vehicle
N87-TR3 + trastuzumab
N87-TR4 + vehicle
N87-TR4 + trastuzumab

Figure 2.

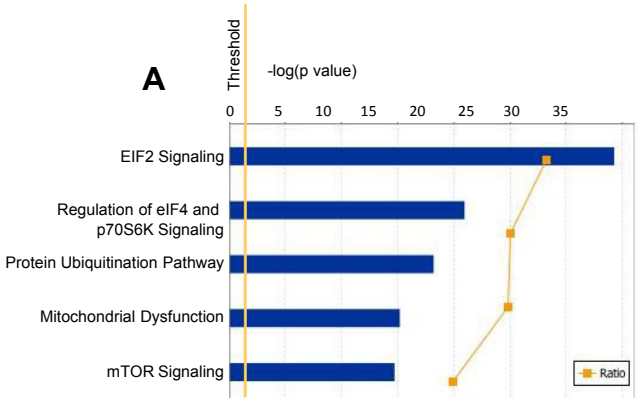
A
Threshold
-log(p value)
0
5
10
15
20
25
30
35
EIF2 Signaling
Regulation of eIF4 and p70S6K Signaling
Protein Ubiquitination Pathway
Mitochondrial Dysfunction
mTOR Signaling
Ratio

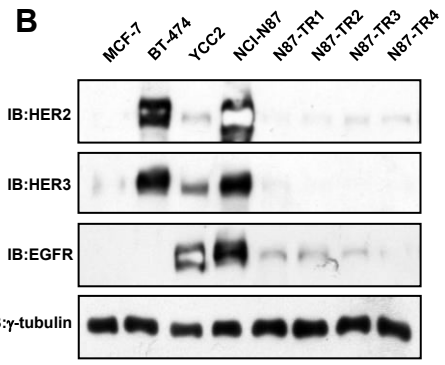
B
MCF-7
BT-474
YCC2
NCI-N87
N87-TR1
N87-TR2
N87-TR3
N87-TR4
IB:HER2
IB:HER3
IB:EGFR
IB:γ-tubulin

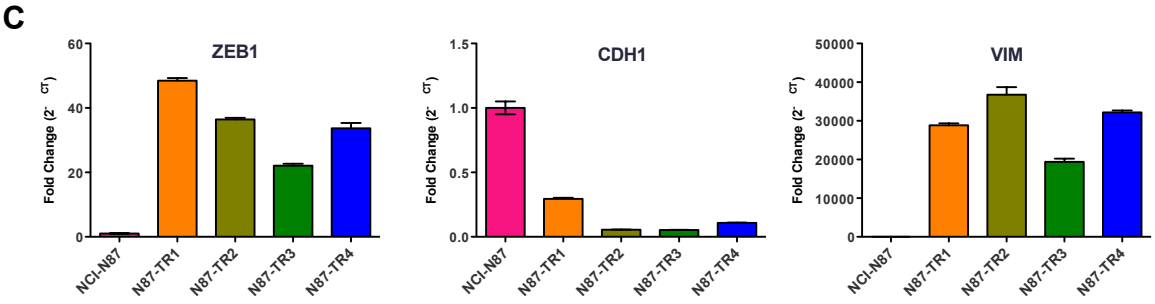
C
ZEB1
CDH1
VIM
Fold Change (2- CT)
NCI-N87
N87-TR1
N87-TR2
N87-TR3
N87-TR4

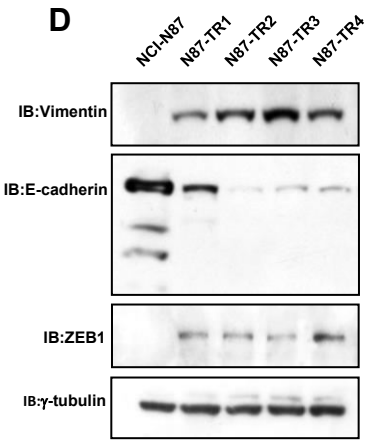
D
NCI-N87
N87-TR1
N87-TR2
N87-TR3
N87-TR4
IB:Vimentin
IB:E-cadherin
IB:ZEB1
IB:γ-tubulin

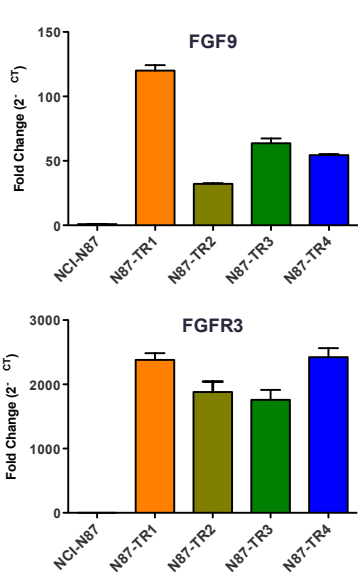
E
FGF9
FGFR3
Fold Change (2- CT)
NCI-N87
N87-TR1
N87-TR2
N87-TR3
N87-TR4

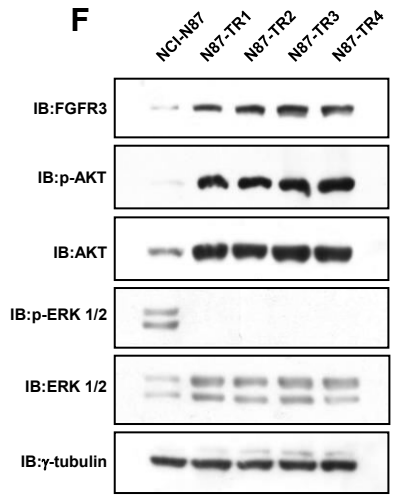
F
NCI-N87
N87-TR1
N87-TR2
N87-TR3
N87-TR4
IB:FGFR3
IB:p-AKT
IB:AKT
IB:p-ERK 1/2
IB:ERK 1/2
IB:γ-tubulin

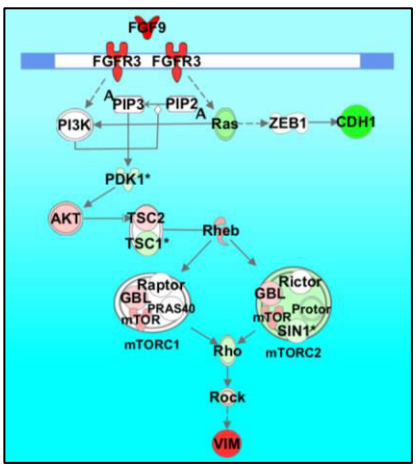
G
FGF9
FGFR3
FGFR3
PIP3
PIP2
PI3K
Ras
ZEB1
CDH1
PDK1*
AKT
TSC2
TSC1*
Rheb
Raptor
GBL
PRAS40
mTOR
mTORC1
Rictor
GBL
mTOR
Protor
SIN1*
mTORC2
Rho
Rock
VIM

Figure 3.

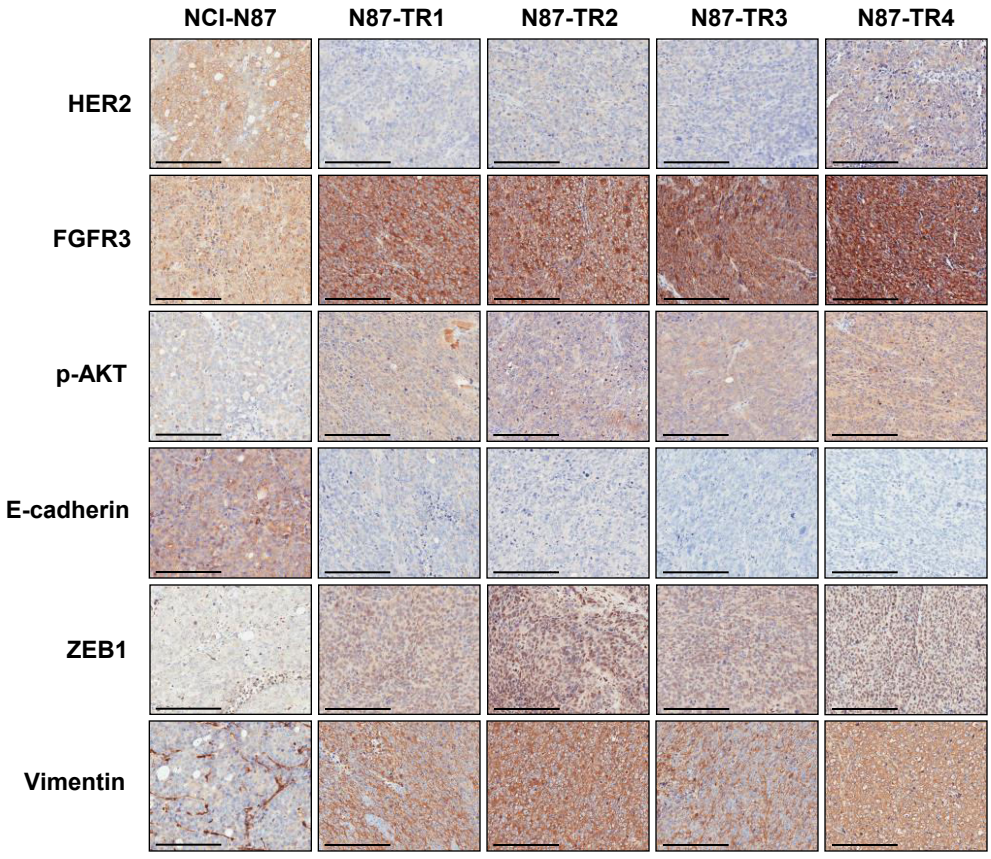
NCI-N87
N87-TR1
N87-TR2
N87-TR3
N87-TR4
HER2
FGFR3
p-AKT
E-cadherin
ZEB1
Vimentin

Figure 4.

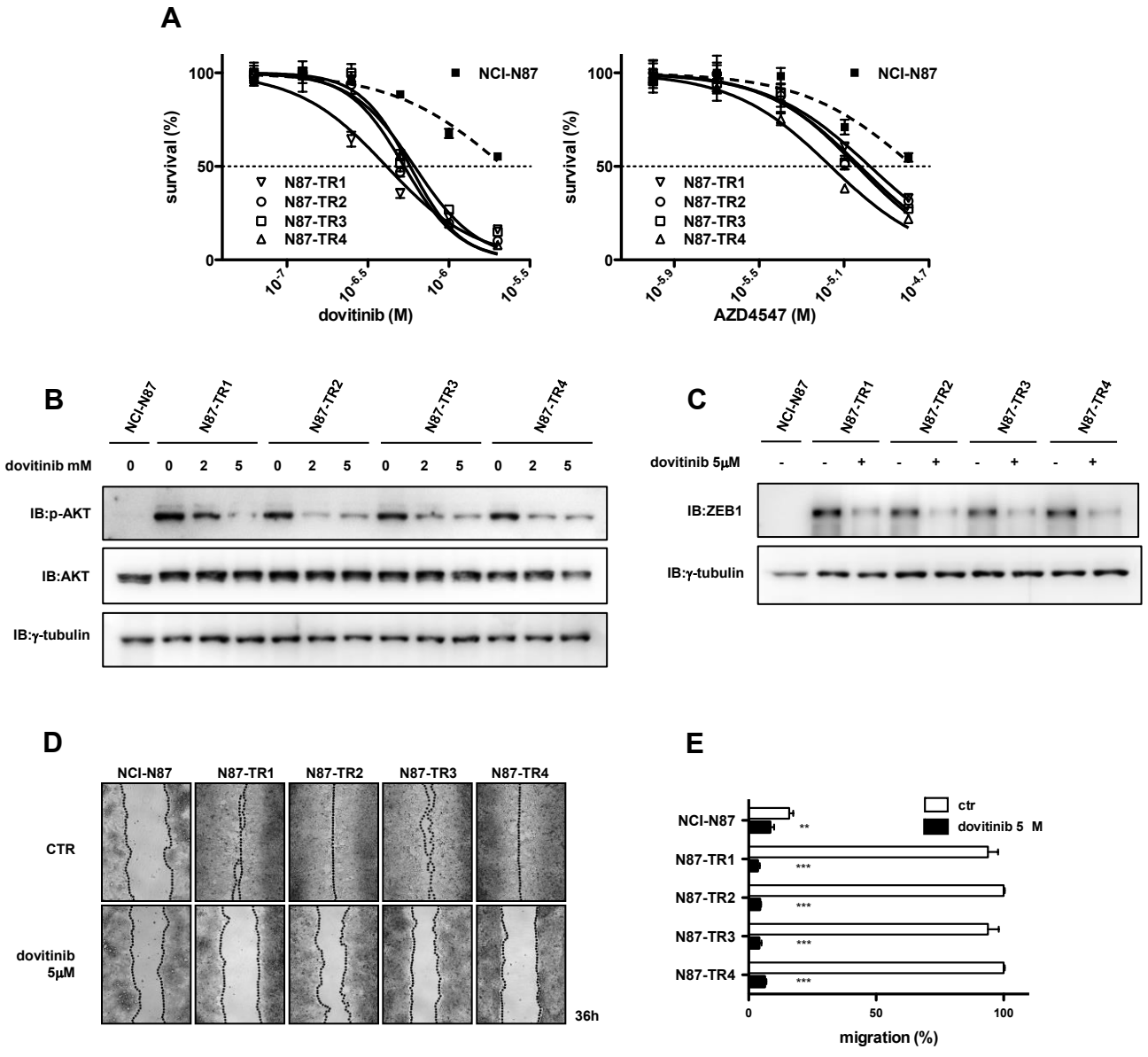
A
survival (%)
100
50
0
NCI-N87
N87-TR1
N87-TR2
N87-TR3
N87-TR4
10-7
10-6.5
10-6
10-5.5
dovitinib (M)
10-5.9
10-5.5
10-5.1
10-4.7
AZD4547 (M)
B
NCI-N87
N87-TR1
N87-TR2
N87-TR3
N87-TR4
dovitinib mM
0 0 2 5 0 2 5 0 2 5 0 2 5
IB:p-AKT
IB:AKT
IB:γ-tubulin
C
dovitinib 5μM
- - + - + - + - +
IB:ZEB1
IB:γ-tubulin
D
CTR
dovitinib 5μM
36h
E
ctr
dovitinib 5 M
**
***
migration (%)

Figure 5.

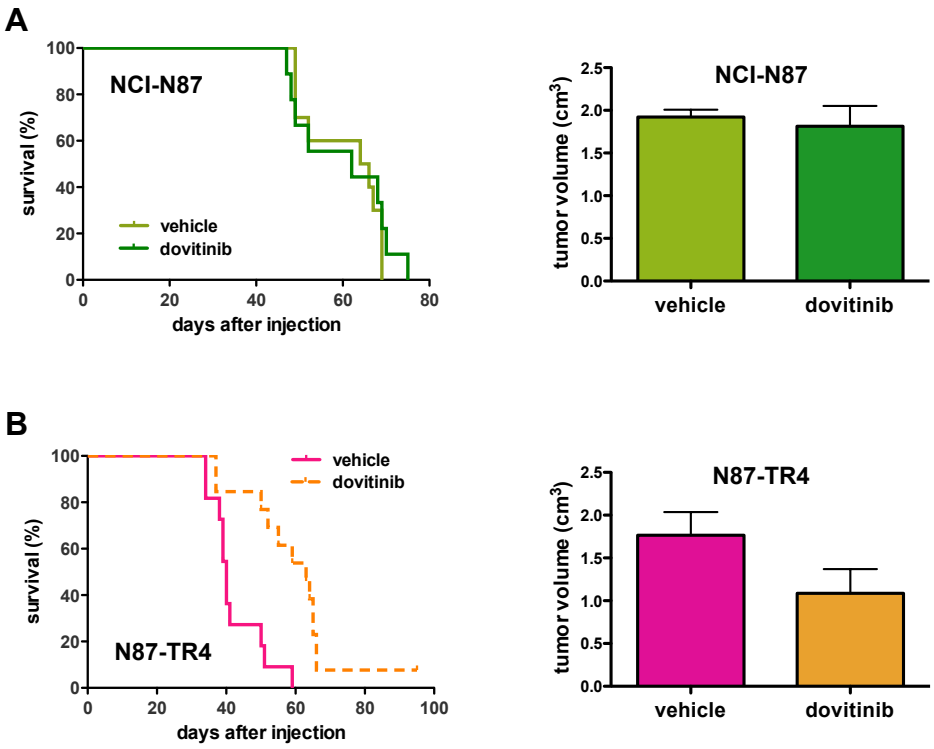
A
NCI-N87
survival (%)
vehicle
dovitinib
days after injection
NCI-N87
tumor volume (cm3)
vehicle
dovitinib
B
N87-TR4
survival (%)
vehicle
dovitinib
days after injection
N87-TR4
tumor volume (cm3)
vehicle
dovitinib

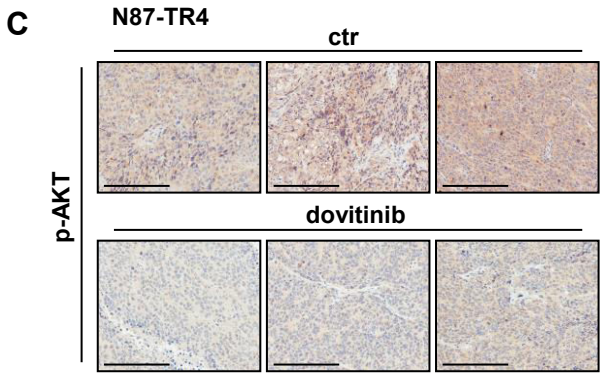
C
N87-TR4
ctr
dovitinib
p-AKT

Figure 6.

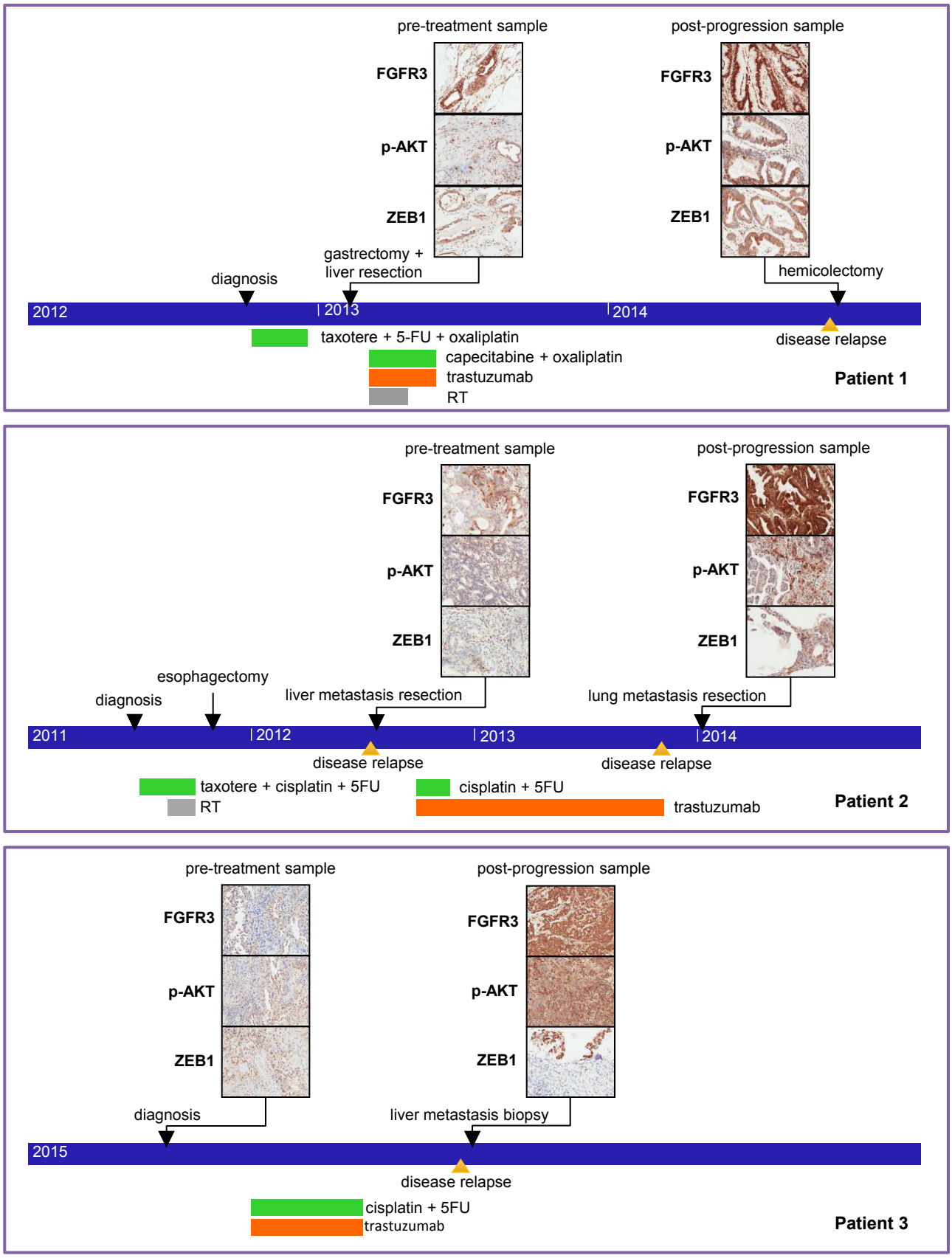
pre-treatment sample
post-progression sample
FGFR3
p-AKT
ZEB1
FGFR3
p-AKT
ZEB1
gastrectomy +
liver resection
hemicolectomy
diagnosis
2012
2013
2014
taxotere + 5-FU + oxaliplatin
capecitabine + oxaliplatin
trastuzumab
RT
disease relapse
Patient 1
pre-treatment sample
post-progression sample
FGFR3
p-AKT
ZEB1
FGFR3
p-AKT
ZEB1
esophagectomy
diagnosis
liver metastasis resection
lung metastasis resection
2011
2012
2013
2014
disease relapse
disease relapse
taxotere + cisplatin + 5FU
RT
cisplatin + 5FU
trastuzumab
Patient 2
pre-treatment sample
post-progression sample
FGFR3
p-AKT
ZEB1
FGFR3
p-AKT
ZEB1
diagnosis
liver metastasis biopsy
2015
disease relapse
cisplatin + 5FU
trastuzumab
Patient 3

Figure S1.

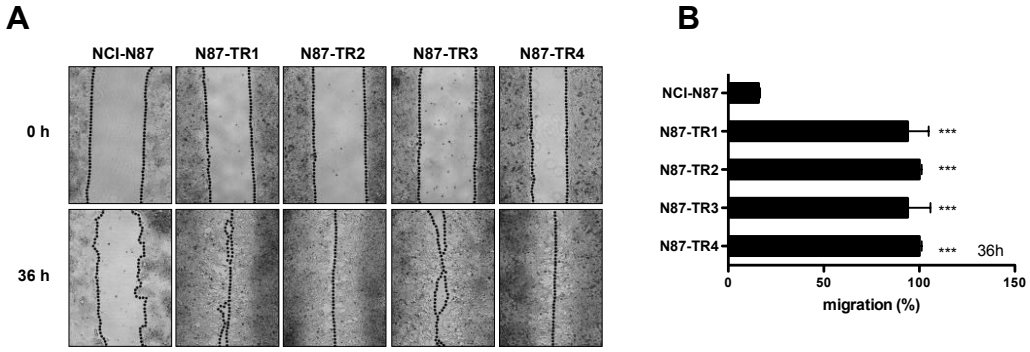

Supplementary Figure 1. Trastuzumab-resistant cells showing features of malignant progression. **A)** Representative photographs of the wound area were taken by using phase-contrast microscopy immediately and 36 hours after the incision. **B)** Differential cell migration between trastuzumab-resistant and –sensitive cells. Results are presented as percentages of the total distances between the wound edges enclosed by cancer cells. The mean values and 95% CIs from 3 independent experiments done in quadruplicate are shown. Relative migration: NCI-N87, mean= 15.91, 95%CI 13.1 to 18.71, vs N87-TR1, mean= 93.85 , 95%CI 86.05 to 101.65; N87-TR2, mean= 100 , 95%CI 99.12 to 100.88; N87-TR3, mean= 93.84, 95%CI 85.42 to 102.25; N87-TR4, mean= 100, 95%CI 99.12 to 100.88; all *P*<.001. ***, P < 0.001 (unpaired Student's t test).

Figure S2.

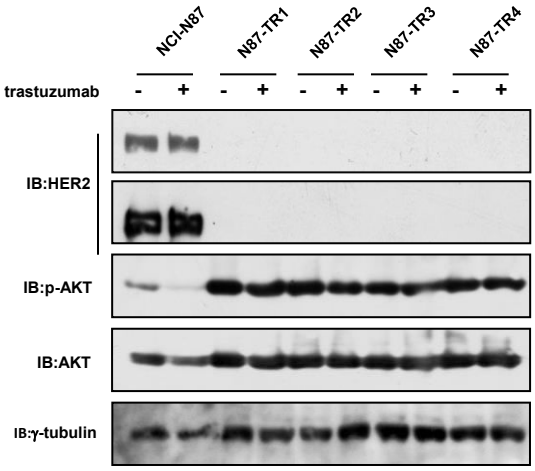

Supplementary Figure 2. Western blot analysis was performed to determine the effect of trastuzumab after 24h of treatment in N87-TR cells and their control cell line.

Supplementary Table 1.

Top-25 up-regulated genes

	Symbol	Probe ID	Entrez Gene Name	Location	Type	Fold-Change N87-TR1	Fold-Change N87-TR2	Fold-Change N87-TR3	Fold-Change N87-TR4
1	VIM	7050019	vimentin	Cytoplasm	O	35.379	51.496	27.501	38.466
2	HSPA1B	3850433	heat shock 70kDa protein 1B	Cytoplasm	E	22.182	21.475	15.573	24.825
3	COCH	4120424	cochlin	Extracellular	O	17.462	22.299	20.363	22.367
4	HSPA1A	6380717	heat shock 70kDa protein 1A	Cytoplasm	E	16.666	15.513	13.278	16.340
5	ZCCHC12	2690279	zinc finger, CCHC domain containing 12	Nucleus	TF	19.187	11.944	17.771	12.844
6	FERMT2	1820328	fermitin family member 2	Cytoplasm	O	10.757	14.146	13.475	12.480
7	IFFO1	6620050	Intermediate filament family orphan 1	Other	O	12.129	11.949	12.458	11.335
8	HES6	610201	hes family bHLH transcription factor 6	Nucleus	TF	12.432	12.274	9.356	11.403
9	SERPINE2	5080192	Serpin peptidase inhibitor, member 2	Extracellular	O	11.790	14.336	8.346	7.795
10	PMAIP1	2750367	phorbol-12-myristate-13-acetate-induced,1	Cytoplasm	O	13.093	10.832	7.931	10.176
11	FGFR3	6520139	Fibroblast growth factor receptor 3	Membrane	K	11.721	8.320	9.750	10.626
12	FLNC	580491	filamin C, gamma	Cytoplasm	O	18.459	7.208	4.141	8.370
13	HOXA9	2810673	homeobox A9	Nucleus	TF	6.080	14.391	8.055	8.322
14	HOXA11AS	5570768	HOXA11 antisense RNA	Other	O	7.479	6.233	16.694	5.944
15	KCTD12	5560500	Potassium channel TD containing12	Membrane	IC	7.783	10.115	5.682	12.397
16	SEPT5	6960022	septin 5	Cytoplasm	E	11.122	7.661	3.558	13.504
17	CA2	870630	Carbonic anhydrase II	Cytoplasm	E	12.387	5.176	7.140	7.970
18	TSC22D3	6350446	TSC22 domain family. member 3	Nucleus	TF	8.878	11.191	2.591	10.002
19	KIF1A	6520440	kinesin family member 1A	Cytoplasm	O	12.051	3.721	10.138	6.596
20	FGF9	6420746	Fibroblast growth factor 9	Extracellular	O	10.450	4.779	8.888	7.664
21	CSRP2	1990152	Cysteine-Rich Protein 2	Nucleus	O	11.190	7.930	5.721	6.924
22	IRX3	5690408	Iroquois homeobox 3	Nucleus	TF	7.661	7.019	6.997	9.997
23	TSC22D3	6350632	TSC22 domain family, member 3	Nucleus	TF	8.104	10.037	4.019	8.947
24	TUBB2B	7050543	Tubuli, Beta 2B Class IIb	Other	O	9.625	7.671	4.550	8.230
25	INSM1	4040474	Insulinoma-Associated 1	Nucleus	TF	13.029	2.757	6.794	6.184

Top-25 down-regulated genes

	Symbol	Probe ID	Entrez Gene Name	Location	Type	Fold-Change N87-TR1	Fold-Change N87-TR2	Fold-Change N87-TR3	Fold-Change N87-TR4
1	NQO1	5360347	NAD(P)H dehydrogenase, quinone 1	Cytoplasm	E	0.015	0.018	0.026	0.020
2	ERBB2	4050156	erb-b2 receptortyrosinekinase2	Membrane	K	0.022	0.030	0.023	0.026
3	FOXQ1	4640086	forkhead box Q1	Nucleus	TF	0.029	0.023	0.024	0.024
4	RPS4Y1	6100687	Ribosomal protein S4, Y-linked 1	Cytoplasm	O	0.032	0.030	0.035	0.030
5	AXIN2	1070189	axin 2	Cytoplasm	O	0.043	0.035	0.045	0.031
6	ANXA1	6520215	annexin A1	Membrane	E	0.046	0.075	0.038	0.020
7	BMP4	990075	Bone morphogenetic protein 4	Extracellular	GF	0.063	0.046	0.050	0.045
8	LOXL4	4150477	Lysyl oxidase-like4	Extracellular	E	0.037	0.066	0.039	0.064
9	MUC1	7650026	mucin 1, cell surface associated	Membrane	TR	0.057	0.055	0.057	0.055
10	PGAP3	2000441	post-GPI attachment to proteins 3	Cytoplasm	E	0.038	0.061	0.072	0.056
11	SLC2A1	4590370	Solute carrier family 2 (member 3)	Membrane	T	0.055	0.047	0.065	0.062
12	TNS3	5560561	tensin 3	Membrane	P	0.049	0.061	0.068	0.052
13	GJC2	6520356	Gap junction protein, gamma 2	Membrane	IC	0.045	0.045	0.085	0.056
14	CTGF	5690687	Connective tissue growth factor	Extracellular	GF	0.047	0.082	0.061	0.061
15	TACSTD1	4070575	Tumor-Associated Calcium Signal Transducer 1	Cytoplasm	O	0.081	0.038	0.043	0.098
16	MPZL2	3890228	Myelin protein zero-like2	Membrane	O	0.054	0.046	0.084	0.075
17	CDH1	1300113	cadherin 1, type 1	Membrane	O	0.129	0.046	0.037	0.059
18	BCL2L1	670673	BCL2-like 12 (proline rich)	Nucleus	O	0.059	0.057	0.104	0.063
19	EPCAM	1690553	Epithelial cell adhesion molecule	Membrane	O	0.096	0.040	0.045	0.113
20	SYTL2	6760037	synaptotagmin-like 2	Cytoplasm	T	0.097	0.065	0.068	0.070
21	FAM83H	1300392	family with sequence similarity 83, H	Other	O	0.049	0.064	0.111	0.079
22	PRAGMIN	2640441	Tyrosine-Protein Kinase SgK223	Cytoplasm	K	0.068	0.086	0.063	0.090
23	ARHGAP23	4210630	Rho GTPase activating protein23	Cytoplasm	O	0.066	0.077	0.097	0.068
24	LASP1	620300	LIM And SH3 Protein 1	Cytoplasm	O	0.085	0.072	0.062	0.095
25	EMP1	3940435	Epithelial membrane type 1	Membrane	O	0.114	0.075	0.070	0.095

Supplementary Table 1. Top differentially regulated coding genes in N87-TR1, N87-TR2, N87-TR3, and N87-TR4 trastuzumab–resistant gastric cancer cell lines compared with NCI-N87 control cell line. TF, Transcriptional Factor; E, Enzyme; K, Kinase; T, Transporter; IC, Ion Channel; TR, Transmembrane Receptor; GF, GrowthFactor; K, Kinase; P, Phosphatase; O, Other. ($P<0.001$).

Supplementary materials and methods – FGFR3 in trastuzumab-resistant gastric cancer

Cell Lines and Reagents

Human gastric cancer cell line NCI-N87 and human breast cancer cell lines MCF-7 and BT474 were obtained from the American Type Culture Collection (Manassas, VA, USA). Human gastric cancer cell line YCC-2 was obtained from Korea Cell Line Bank (KCLB, Seoul, Korea). Cell lines were authenticated by standard short tandem repeat (STR) DNA typing methodology before being purchased from cell bank. Cells were daily checked by morphology and routinely tested to be Mycoplasma free by PCR assay. All cell lines were maintained in Roswell Park Memorial Institute (RPMI) 1640 medium or Dulbecco's Modified Eagle Medium (DMEM) (Lonza, Verviers, Belgium), supplemented with 10% heat-inactivated FBS, 20 mmol/L HEPES (pH 7.4), penicillin (100 UI/mL), streptomycin (100 mg/mL), and 4 mmol/L glutamine (ICN Biomedicals Ltd.) in a humidified atmosphere of 95% air and 5% CO2 at 37°C. Fibroblast growth factor receptor 3 (FGFR3) inhibitors dovitinib (TKI-258) and AZD4547 were purchased from Selleck Chemicals (London, ON, Canada). For in vitro assays, dovitinib was dissolved in 100% dimethyl sulfoxide (DMSO) at a stock concentration of 10 mM. The concentration of DMSO did not exceed 0.1% in any assay. For in vivo studies, dovitinib was dissolved in saline at a stock concentration of 50 mg/ml and administered by oral gavage. Monoclonal antibody trastuzumab (Herceptin®) was obtained from the local hospital pharmacy.

Generation of lentivirus

Green fluorescent protein+/luciferase+ NCI-N87 cell line was obtained by lentiviral infection. Lentivirus was produced by transient cotransfection into the human 293T cell line with appropriate transfer and lentiviral helper plasmids (pCMV/PRARE packaging vector and pMD2.VSVG envelope vector) using LT1-mirus according to manufacturer method. 18 hours later, growth media (DMEM containing 10% Fetal

Bovine Serum and 1% penicillin/streptomycin) were changed. Lentiviral supernatant was harvested at 48 h and 72 h post transfection and filtered through a 0.45-μm filter. Lentiviral supernatants were concentrated 20- fold by ultracentrifugation at 4°C for 10 h at 10,000 g. Harvested lentiviruses were stored at -80°C. To assess the activity of virus encoding the firefly-luciferase reporter gene, the human 293T cells were infected by adding thawed lentivirus-containing supernatant at a final concentration of 8 g/ml Polybrene (Sigma, St. Louis, Missouri, USA). Luciferase expressions were confirmed by determining luciferase activities using a luminometer (Applied Biosystems, Forster, CA) and GFP co-expression was assessed by fluorescence microscopy.

Cell Proliferation Assay to Determine Sensitivity to Trastuzumab and Dovitinib

On day 0, 1.0 x 10^3 cells/well were seeded in 96-well plates. On the following day, the cells were treated with increasing doses of trastuzumab or dovitinib. After 72 hours of incubation, sulforhodamine B (SRB) (Sigma, St. Louis, Missouri, USA) assay was used to obtain relative estimates of viable cell number. Briefly, trichloroacetic acid fixed cells were stained for 30 minutes with 0.4% SRB dissolved in 1% acetic acid. At the end of the staining incubation, SRB was removed and cultures were quickly rinsed four times with 1% acetic acid to remove unbound dye. After being rinsed, the cultures were air dried until no standing moisture was visible. Bound dye was resuspended in Tris 10mM pH 10,5 and read with iMark Microplate Absorbance Reader spectrophotometer (Hercules, California, USA) at 540 nm.

Protein extraction and western blotting

Cell lines were washed twice with cold phosphate-buffered saline and lysed at 4°C into radioimmunoprecipitation assay buffer (50 mM Tris–HCl [pH 8], 150 mM NaCl, 1% Nonidet P-40, 0.5% sodium deoxycholate, and 0.1% sodium dodecyl sulfate)

plus protease inhibitor mix, (50 nM sodium pyrophosphate, 0,5 mM sodium orthovanadate, 50 mM NaF, 5 □g/ml Aprotinin, 0.5 mM PMSF (Fenilmetilsulfonil hydrofluoride), 1 mM DTT, 2 μg/mL Leupeptin, 5 μg/mL Benzamidine, 1 μg/mL Pepstatine. Lysates were clarified by centrifugation and protein concentrations were determined by BCA assay (Thermo Scientific). Each lysate was separated by sodium dodecyl sulfate-polyacrylamide gel electrophoresis and probed (1:1000) with rabbit monoclonal antibodies against E-Cadherin, FGFR3 (Abcam, Cambridge, UK), Phospho ERK 1/2 (Thr202/204), TCF8/ZEB1 (Cell Signaling Technology, Boston, MA), mouse monoclonal antibodies against vimentin (Dako, Denmark), rabbit polyclonal antibodies against γ-tubulin, HER3 (Santa Cruz Biotechnology, Santa Cruz, CA), HER2, EGFR, Akt, Phospho-Akt (ser473), ERK 1/2 (Cell Signaling Technology, Boston, MA). Immunoreactive proteins were detected using an enhanced chemiluminescence reagent (ECL, Millipore, Billerica, MA) according to the manufacturer's instructions. Images were captured either on film or by LAS4000 Digital Image Scanning System (GE Healthcare, Little Chalfont, UK).

Gene Expression Microarray and Pathway Analysis

Total RNA was obtained from cells using Trizol reagent (Ambion, Warrington, UK) and following the procedures outlined by the supplier. The quality of RNA was determined by electrophoresis on agarose gel and staining with ethidium bromide, the 18S and 28S bands were visualized by ultraviolet light. Total RNA was quantified by absorbance at 260 nm. Differences in gene expression between parental NCI-N87 and resistant N87-TR cells were examined using Illumina Human 48k gene chips (Illumina, Milan, Italy). Briefly, synthesis of cDNA and biotinylated cRNA was performed using the IlluminaTotalPrep RNA Amplification Kit (Ambion), according to the manufacturer's protocol using 500ng of total RNA. Hybridization of cRNAs (750 ng) was carried out using Illumina Human 48k gene chips (Human HT-12 V4 BeadChip). Array washing was performed using Illumina High Temp Wash Buffer for

10’ at 55°C, followed by staining using streptavidin-Cy3 dyes (Amersham Biosciences). Probe intensity data were obtained and normalized using cubic spline by the Illumina Genome Studio software (Genome Studio V2011.1). Each microarray experiment was repeated twice. Differentially expressed transcripts were tested for network and functional interrelatedness using the IPA software program (Ingenuity Systems, Redwood, CA). Gene expression microarray data have been deposited in the GEO database (accession number GSE77346).

RNA Isolation and Quantitative RT-PCR Assay

Total RNA was isolated by Trizol reagent as indicated by the manufacturer’s instructions (Invitrogen, Carlsbad, CA, USA). The quality and integrity of the RNA were confirmed by agarose gel electrophoresis and ethidium bromide staining, followed by visual examination under UV light. Reverse transcription was performed using the High Capacity Reverse Transcription Kit (Qiagen, Venlo, Netherlands). The cDNA obtained was evaluated for Real-Time PCR with ABI Prism 7900 HT Sequence Detection System (Applied Biosystems, Foster City, CA, USA) using specific primer and SYBR Green probe. QuantiTect Primer Assays (Qiagen, Venlo, Netherlands) were used to quantify cDNA levels of CDH1 (Hs_CDH1_1_SG), VIM (Hs_VIM_1_SG), and beta actin (Hs_ACTB_2_SG). Validated All-in-One^{TM} qPCR Primers (Gene Copoeia Inc., Rockville, MD, U.S.A) were used to quantify cDNA levels of FGF9 (HQP054307) and FGFR3 (HQP005434). Each sample was assayed in triplicate with 30 ng of input cDNA per well in a volume of 25 μl reaction containing QuantiTect SYBR Green PCR Master Mix and specific primers. Specificity of the produced amplification product was confirmed by examination of dissociation reaction plots. Cycle threshold values (Ct) generated from Sequence Detection System 2.2.2 (Applied Biosystems, Foster City, CA, USA) were exported to determine relative cDNA abundances among genes. Gene expression was calculated using $2^{-\Delta\Delta CT}$ method and normalized to β-actin expression.

Establishment of Gastric Cancer Cell Lines In Vivo Resistant to Trastuzumab

Six- to eight-week-old female BALB/c athymic (nu/nu) mice were purchased from Harlan Laboratories (Indianapolis, Indiana). All of the mice were housed and given treated in Animal Care Facility of CIRSAL (Verona, Italy) in accordance with the guidelines of the Italian Ministry of Health Animal Care and Use Committee, and maintained in specific pathogen-free conditions. For orthotopic implantation, green fluorescent protein+/luciferase+ NCI-N87 cell line was harvested from sub-confluent culture by exposure to trypsin. Trypsinization was stopped with medium containing 10% Fetal Bovine Serum, and the cells were washed once with Phosphate Buffered Saline (PBS). To produce orthotopic gastric tumors, $1x10^6$ cells resuspended in 50 µl of PBS/matrigel solution (1:1) were injected into the gastric wall of six nude mice anesthetized with a 1.5% isoflurane–air mixture. To prevent such leakage, a cotton swab was held over the injection site for 1 minute. One layer of the abdominal wound was closed with wound clips (Auto-clip; Clay Adams, Parsippany, NJ). The mice tolerated the surgical procedure well, and no anesthesia-related deaths occurred. Tumor growth was monitored by Bioluminescent imaging performed using a cryogenically cooled IVIS 100 imaging system coupled with a data-acquisition computer running the Living Image software program (Xenogen, Hopkinton, MA). When the resulting tumors became detectable, the mice were given 20 mg/kg of trastuzumab intraperitoneally (i.p.) twice a week until the tumors suddenly recurred during continuous therapy. Treatment resistance developed in 4 out of 6 mice. At evidence of advanced bulky disease, mice were euthanized using carbon dioxide inhalation. Four trastuzumab-resistant cell lines were established from excised tumors via repeated green fluorescent protein flow cytometric sorting with FACSAria II sorter (Becton Dickinson, Franklin Lakes, New Jersey, USA).

In Vivo Antitumor Activity of Trastuzumab or Dovitinib in Gastric Tumor Xenografts

Tumor bearing mice were randomly assigned (n = 10 per group) to receive 20mg/Kg of trastuzumab i.p. twice a week for four weeks, or 40 mg/kg of dovitinib oral gavage daily for four weeks, or respective vehicles as a control. Tumor size was measured with a caliper by the modified ellipsoid formula $(\pi/6) \times AB^2$ where A is the longest and B is the shortest perpendicular axis of an assumed ellipsoid corresponding to tumor mass. All mice were weighed weekly and observed for tumor growth. When at least six of the ten mice in a treatment group presented with bulky disease, the median survival duration for that group was considered to have been reached. At the median survival duration of the control group, the tumor growth in mice in all groups was evaluated. The mice were euthanized using carbon dioxide inhalation when evidence of advanced bulky disease developed or at cut-off volume of 2 cm^3, which was considered the day of death for the purpose of survival evaluation.

Wound Healing assay

NCI-N87 and resistant N87-TR cells were seeded to 90% of confluence in 100mm cell culture dishes. After 24 hours cells were treated with 5μM of dovitinib or DMSO as control, a straight scratch was made using a pipette tip to simulate a wound. The cells were washed gently with cold PBS1X and rinsed with fresh medium. Photographs at five different points at least were taken immediately and after 36 hours of culture.

Patients

Three patients were considered for analyses. Patient 1 was a 62 year-old man diagnosed in October 2012 with a locally advanced gastric cancer infiltrating pancreatic head as well as IV segment of liver. The patient received three courses of

neo-adjuvant chemotherapy with oxaliplatin, 5-fluorouracil and docetaxel. In January 2013, the patient underwent total gastrectomy and atipical liver resection. Pathology revealed a gastric adenocarcinoma, G2, intestinal histotype sec. Lauren, tubular and mucinous according to WHO classification (ypT4b N0/27 M0, HER-2: score 3; pre-treatment sample). Thereafter, he received systemic chemotherapy with trastuzumab, oxaliplatin, capecitabine associated with radiotherapy. In October 2014, the patient developed peritoneal metastases, thus he underwent laparotomy and right hemicolectomy. Pathology revealed a poorly differentiated adenocarcinoma with gastric origin; HER-2: score 1 (post-progression sample).

Patient 2 was a 63-year-old man diagnosed in July 2011 with a locally advanced Siewert type II esophagogastric junction adenocarcinoma with multiple regional lymph node metastases (cT3 N+ M0). Patient received neoadjuvant chemo-radiotherapy with docetaxel, cisplatin, and fluorouracil as previously described (BJC). In November 2011, the patient underwent sub-total esophagectomy (Ivor-Lewis procedure). At pathological examination there was no evidence of residual carcinoma in the resected specimen and no evidence of metastasis in the 31 retrieved lymph nodes (ypT0 N0/ 31 M0, TRG= 1 sec. Mandard,). No adjuvant treatment was administered. In March 2012, the patient underwent resection of a single liver metastases (pre-treatment sample). Histology confirmed adenocarcinoma of gastric origin, HER-2: score 3 (pre-treatment sample). Thus, the patient received chemotherapy with cisplatin and 5-fluorouracil for 3 cycles associated with continuous trastuzumab. In December 2013, CT scan showed a new single lung metastasis. In January 2014, the patient underwent toracoscopic atipical lung resection. Pathology revealed an adenocarcinoma metastasis of gastric origin (post-treatment sample).

Patient 3 was a 57 year-old man diagnosed in January 2015 with an advanced esophagogastric junction adenocarcinoma with multiple liver and lung metastases (cT3N1M1, HER-2: score 3) (pre-treatment sample). The patient received first-line

chemotherapy with cisplatin and 5-fluorouracil associated with trastuzumab. In May 2015, CT scan showed liver disease progression. New biopsy was performed, confirming liver progression of esophagogastric junction adenocarcinoma (post-treatment sample).

For each patient, pre- and post-resistance tumor samples were compared by immunohistochemical analyses. Informed consent was obtained from all patients.

Immunohistochemistry

Six mice bearing N87-TR4 gastric tumors were randomly allocated (n= 3 per group) to receive 40 mg/kg daily oral dovitinib or vehicle as control. Treatments were continued for 4 weeks. Tumors were excised 1 day after the end of treatments. Formalin-fixed paraffin-embedded 4 µm tissue sections were incubated at 4°C over night with the following rabbit anti-human primary antibodies, according to the manufacturer's instructions: anti-HER2 (HercepTest , Dako Autostainer kit, code K5207), anti-FGFR3 (clone ab137084, 1:100; Abcam, Cambridge, UK), anti-ZEB1 (clone ab87280, 1:250, Abcam, Cambridge, UK), anti-pAKT- S473 (1:100, Abcam, Cambridge, UK), anti-E-cadherin (clone EP700Y, 1:500; Abcam, Cambridge, UK), and anti-Vimentin (clone EPR3776, 1:200; Abcam, Cambridge, UK), Slides were washed in Tris-buffered saline buffer and then incubated for 30 minutes with the appropriate horseradish peroxidase–conjugated secondary antibody. Color was detected with VECTASTAIN ABC Kit Rabbit IgG (Novocastra, Leica Microsystems, Wetzlar, Germany) for xenograft, tissue or with HRP Anti-Rabbit IgG Polymer Detection Kit (Novocastra, Leica Microsystems, Wetzlar, Germany) for human tissue. The slides were counterstained with Meyer's hematoxylin (Peroxidase Detection System; Leica Microsystems Inc., Wetzlar, Germany). To ensure antibody specificity, consecutive sections were incubated with isotype-matched control immunoglobulins and in the absence of the primary antibody. In these cases, no specific immunostaining was detected. The expression of proteins was detected as

membrane, cytoplasmic or nuclear brown staining of varying intensity in neoplastic cells. The slides were evaluated independently using light microscopy by two pathologists who were blinded to the treatments.

Statistical Analysis

The results of in vitro proliferation were analyzed for statistical significance of differences by nonlinear regression analysis and are expressed as means and 95% confidence intervals [CIs] for at least three independent experiments performed in quadruplicate. The statistical significance of differences in tumor growth was determined by the Mann–Whitney test; differences in survival duration were determined using a log-rank test. All statistical tests were two-sided, and a P value less than .05 indicated statistical significance. All statistical analyses were performed using GraphPad Prism software version 4.0c for Macintosh (GraphPad Software, San Diego, CA).